Determination of tungsten sources in the JET-ILW divertor by spectroscopic imaging in the presence of a strong plasma continuum

Nuclear Materials and Energy 18 (2019) 118–124

Contents lists available at ScienceDirect

Nuclear Materials and Energy

journal homepage: www.elsevier.com/locate/nme

Determination of tungsten sources in the JET-ILW divertor by spectroscopic imaging in the presence of a strong plasma continuum

A. Huber[a,*], S. Brezinsek[a], A. Kirschner[a], P. Ström[b], G. Sergienko[a], V. Huber[c], I. Borodkina[a,d], D. Douai[e], S. Jachmich[f], C.h. Linsmeier[a], B. Lomanowski[g], G.F. Matthews[h], P.h. Mertens[a], JET contributors[1,i]

[a] Forschungszentrum Jülich GmbH, Institut für Energie- und Klimaforschung - Plasmaphysik, 52425 Jülich, Germany
[b] Department of Fusion Plasma Physics, Royal Institute of Technology (KTH), 10044 Stockholm, Sweden
[c] Forschungszentrum Jülich GmbH, Supercomputing Centre, 52425 Jülich, Germany
[d] National Research Nuclear University MEPhI, 31, Kashirskoe sh., Moscow, Russia
[e] CEA, IRFM, F-13108St-Paul-Lez-Durance, France
[f] Laboratory for Plasma Physics, ERM/KMS, B-1000 Brussels, Belgium
[g] Aalto University, Otakaari 4, 02015 Espoo, Finland
[h] CCFE, Culham Science Centre, Abingdon, OX14 3DB, UK
[i] EUROfusion Consortium, JET, Culham Science Centre, Abingdon, OX14 3DB, UK

ARTICLE INFO

Keywords:
Tungsten erosion
Tungsten imaging spectroscopy
W Divertor
JET-ILW
PSI
PFC

ABSTRACT

The identification of the sources of atomic tungsten and the measurement of their radiation distribution in front of all plasma-facing components has been performed in JET with the help of two digital cameras with the same two-dimensional view, equipped with interference filters of different bandwidths centred on the W I (400.88 nm) emission line. A new algorithm for the subtraction of the continuum radiation was successfully developed and is now used to evaluate the W erosion even in the inner divertor region where the strong recombination emission is dominating over the tungsten emission. Analysis of W sputtering and W redistribution in the divertor by video imaging spectroscopy with high spatial resolution for three different magnetic configurations was performed. A strong variation of the emission of the neutral tungsten in toroidal direction and corresponding W erosion has been observed. It correlates strongly with the wetted area with a maximal W erosion at the edge of the divertor tile.

1. Introduction

Tungsten (W) is foreseen as the main plasma-facing material (PFM) in fusion devices, such as ITER with full-tungsten divertor [1,2], because of its excellent material properties − a high threshold energy for sputtering [3], a high melting point [4] and a low tritium inventory [5,6]. The tungsten concentration in the core plasma has to be controlled and kept below $\approx 3 \times 10^{-5}$ [7] to avoid large central radiation losses. Therefore, it is very important to get a complete understanding of the critical parameters for the erosion of tungsten components, particularly in the divertor and to find the recipe to control the W source. The knowledge of the W-erosion distribution in the divertor, which can be provided by video imaging spectroscopy, is especially important. However, the relatively weak line radiation emitted by neutral tungsten, the W I emission, is often masked by the presence of the plasma continuum radiation (free-free, free-bound) and thermal radiation from the hot surfaces.

Fig. 1 shows the relative contributions of the continuum free-free, free-bound and thermal spectral radiance given a 2 m thick homogenous deuterium plasma without impurity seeding.

During monitoring pulses without impurity seeding in the JET ITER-like Wall (JET-ILW) an average $Z_{eff} = 1.6$ for all plasma scenarios is observed [8]. We consider here the most critical case with strong bremsstrahlung level, assuming $Z_{eff} = 2.0$.

The bremsstrahlung intensity as well as the free-bound hydrogenic intensity were calculated using ADAS [9]. Plasma parameters for these estimates were chosen to determine typically high and low levels of bremsstrahlung. The high density ($10^{20}\,m^{-3}$), low electron temperature case ($T_e = 5$ eV) represents the semi-detached plasma conditions whereas low density ($2 \times 10^{19}\,m^{-3}$) and high electron temperature

* Corresponding author.
E-mail address: a.huber@fz-juelich.de (A. Huber).
[1] See the author list of "X. Litaudon et al 2017 Nucl. Fusion 57 102001"

https://doi.org/10.1016/j.nme.2018.12.009
Received 8 August 2018; Received in revised form 6 December 2018; Accepted 7 December 2018
Available online 18 December 2018

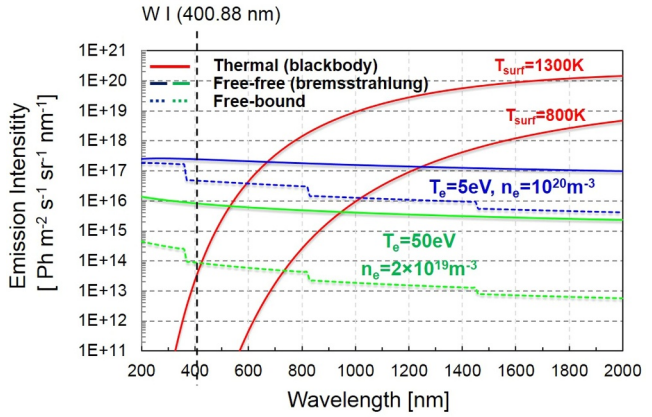

Fig. 1. Calculated continuum emission spectrum contributions from Bremsstrahlung, radiative recombination and thermal emission for a 2 m thick isotropic deuterium plasma without impurity seeding. An effective charge of $Z_{eff} = 2.0$ is assumed.

($T_e = 50$ eV) are typical parameters for the attached divertor on JET-ILW.

The thermal emission was calculated using Planck's blackbody emissivity formula for two surface temperatures, $T_{surf} = 800$ K and $T_{surf} = 1300$ K. For surface temperatures below 1300 K the bremsstrahlung as well as the free-bound emission will dominate in the spectral range around 400 nm. It is mainly bremsstrahlung that has a significant impact on the WI emission measurements. W sources were studied in the JET-ILW environment with optical emission spectroscopy by monitoring the WI line radiation at 400.9 nm in the outer divertor. It was found [10] that intra-ELM erosion dominates the total W source with intra-ELM and inter-ELM W fluxes of 0.7–1.0 $\times 10^{20}$ m^{-2} s^{-1} and 1–4 $\times 10^{19}$ m^{-2} s^{-1} respectively (JPN 82237, 13 MW NBI heating power, 7.5 $\times 10^{19}$ m^{-3} line averaged n_e, 10 Hz ELMs). The W atom influxes were calculated by using the following formula [11,12]:

$$\Gamma_W = 4\pi \frac{S}{XB}(T_e)\cdot I_{WI}, \quad (1)$$

where I_{WI} is the measured photon flux of the WI emission line and the *S/XB* multiplication factor is the so-called inverse photon efficiency or the number of ionizations per photon. For the WI-line at 400.88 nm, the *S/XB* -factor is intensively discussed in [10,13,14]. Similarly to [10], taking the *S/XB* values of 30 (15) for the intra (inter) ELM phase, we get measured photon fluxes of the WI emission line: 1.8–2.7 $\times 10^{17}$ ph/m^2 s^{-1} sr^{-1} for intra-ELM and 0.5–2.1 $\times 10^{17}$ ph/m^2 s^{-1} sr^{-1} for inter-ELM phases. More recently measured values of *S/XB* on TEXTOR [14] are 9 and 45 for the $T_e = 5$ eV and $T_e = 50$ eV respectively corresponding to the WI emission photon flux range 0.2–3.5 $\times 10^{17}$ ph/m^2 s^{-1} sr^{-1} for inter-ELM phase. Taking into account the Full Width at Half Maximum (FWHM) of the used bandwidth filter of 1 nm, the estimated bremsstrahlung is ~10^{16} ph/s m^{-2} sr^{-1} for the attached divertor ($T_e = 50$ eV, $n_e = 2 \times 10^{19}$ m^{-3}) and ~2×10^{17} ph/s m^{-2} sr^{-1} for the detached plasma conditions ($T_e = 5$ eV, $n_e = 10^{20}$ m^{-3}) (see Fig. 1). The estimated I_{WI} is thus comparable to the calculated bremsstrahlung emission intensity.

It should be mentioned here that the recombination (free-bound) emission disturbs the W I line emission measurements in the completely detached cold divertor ($n_e = 10^{20}$ m^{-3}, $T_e = 1$ eV). Under cold detached divertor with significant reduction of W sputtering, the tungsten is introduced into the plasma only during the ELMs. Under fully detached divertor conditions with high electron densities, the electron density dependence of the WI *S/XB* values may become important [14]. This is also important for the calculation of the W erosion during the ELMs. The electron density dependence of the *S/XB* coefficient has been confirmed recently by studies in DIII-D at high plasma densities [15]. The first experiments in DIII-D demonstrate the increase of the WI *S/XB* coefficients for densities above 10^{19} m^{-3}. However, studies of the electron density dependence of the WI *S/XB* coefficient are outside the scope of this contribution. In this work the multi-machine fit for WI *S/XB* in the experimentally covered range of $T_e = 2$ eV and $T_e = 82$ eV [14] is used. As discussed in [14], this multi-machine fit reproduces well the shape of the corresponding theoretical curve of *S/XB* for WI emission line at 400.9 nm deduced from the ADAS database [9]. The absolute *S/XB* values systematically deviate by about 50% from each other. The most likely reason for the discrepancy are not the electron impact excitation rate coefficients used in ADAS, but the ionisation rate coefficients for W. The experimentally determined ionisation rates revealed a discrepancy when compared with theoretical calculations (ADAS, GKU, and Lotz) [13,14]. More studies are required to resolve this issue.

The first ELM-resolved W source measurement with plasma continuum subtraction is obtained on JET-ILW via a cross-calibration procedure between divertor spectroscopy and photo multiplier tube (PMT) measurements [10]. This method is recognised as a time consuming and complex approach. An additional drawback of this method is that it delivers the space averaged information about the W sources without any spatial resolution. Other methods with background subtraction without spatial resolution have been also developed for the filterscopes on TEXTOR [16] and recently on DIII-D and WEST [17,18]. With respect to spatially resolved measurements, the imaging filtering on JET was based on a single camera measurement using the fact that the background radiation pattern is toroidally symmetric. It allows to discriminate the line emission from the plasma continuum radiation under the assumption that the areas on the image used for plasma continuum measurement are not affected by the emission of the measured spectral lines. A similar approach was proposed in the recently published paper [17]. This approach does not work well for the tangentially viewing imaging system because each camera pixel collects the light along different lines-of-sight and thus has an individual level of plasma background. Additionally, this method is strongly dependent on the magnetic configuration of the plasma scenarios as well as on the correctness of the aforementioned assumptions.

In this contribution, a new method for the subtraction of the continuum radiation for the JET imaging system was successfully developed and is now used to evaluate the W erosion even in the inner divertor region where the strong recombination emission is dominating over the tungsten emission. In the present paper, we will demonstrate the detailed description of the algorithm. Additionally, analysis of W sputtering and W redistribution in the divertor by video imaging spectroscopy with high spatial resolution at JET tokamak, equipped with the ITER-like Wall material configuration [19,20], will be presented.

2. Method for extraction of WI emission line from the imaging spectroscopy

2.1. Basic approach for extraction the WI emission line

The identification of the tungsten atom sources and the measurement of their radiation profiles in front of all plasma-facing components has been performed in JET with the help of a full mirror endoscope [21,22] equipped with four digital monochrome CCD cameras (AVT Pike F-100B fibre), each combined with filter wheels for narrow-band interference and neutral density filters. The cameras are equipped with a Kodak image sensor (KAI-1020) with a maximum resolution of 1000 × 1000 pixels and an effective pixel size of 7.4 μm × 7.4 μm (this area is defined by square micro-lenses located in front of the photodiode). The dynamic range of the sensor is 10 bit, i.e. the contrast ratio that can be captured is about 1000:1, and the camera has an ADC of 14 bit, allowing the full dynamic range to be stored in an image. The sensor is an interline transfer CCD, i.e. it has a light sensitive area

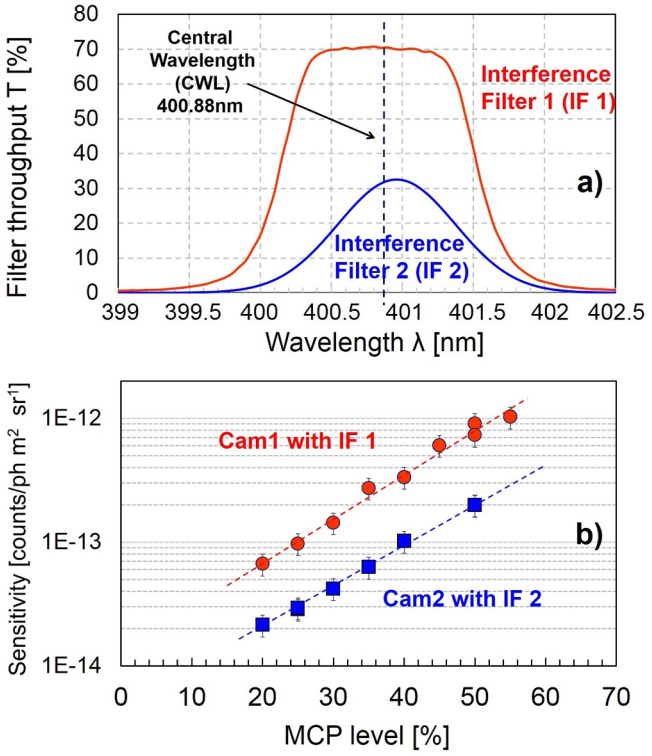

Fig. 2. (a) Transmittance curves of the two bandpass filters used for W I emission record; (b) Measured sensitivity of the intensified camera equipped with an image intensifier 2562 BZ with the WI filters installed in front of the photocathode.

interleaved with a separate storage area, and is equipped with microlenses to effectively increase the light sensitive area. The electronic shutter allows exposure times between 43 μs and ≈67 s and the cameras can operate at a full frame rate of 32.8 Hz (or 59.9 Hz with reduced dynamic range).

Two of the four cameras are equipped with single Multi-channel plate (MCP) image intensifiers (MCP-PROXIFIER) to be able to record spectral lines of low intensity. The intensifier type is BV 2562 BZ, it is optimised for detecting radiation in the wavelength range around 400 nm. The gain of the image intensifier is controlled via the parameter "MCP level" with values in the range of 1%–100% setting the control voltage between 0 V and 5 V which is translated into an MCP output voltage of 400–800 V. The in-vessel calibration of the imaging systems has been performed with the help of integrating spheres coupled to a stable, broad spectrum light source of known radiance [23]. The sensitivity of the imaging systems equipped with intensified cameras has been measured for different levels of MCP and Fig. 2b shows the result for cameras with the WI filter installed in front of the photocathode.

This diagnostic system provides simultaneously the same two-dimensional view for different spectral lines. The usage of interference filters for the spectral imaging of the divertor plasma has a drawback: the essential amount of plasma continuum radiation can pass through the filter due to large difference between the filter bandpass width and the spectral line width and can distort the single spectral line image. The scope of this method is to provide a single spectral line image of the tungsten emission by using two camera images of the same field of view with interference filters (IFs) of different bandwidths and centred on the W I (400.88 nm) emission line (see Fig. 2a).

The detector signal for digital cameras with linear response S_j in fusion devices is a composition of signals due to the spectral photon flux (or photon irradiance) of the detected emission line, L_λ [ph/m^2 s^{-1} sr^{-1} nm^{-1}], and of continuum plasma emission (assumed to be mostly bremsstrahlung), S_{brems} [ph/m^2 s^{-1} sr^{-1} nm^{-1}]:

$$S_j = K_j \times \int L_\lambda \cdot \tau_j(\lambda) d\lambda + K_j \times \int S_{brems}(\lambda) \cdot \tau_j(\lambda) d\lambda \quad (2)$$

Here K_j is a constant for a given detector system (j = 1,2) at given λ and represents the calibration factor, L_λ is the spectral photon flux of the respective emission line, W I (λ_0=400.88 nm), $\tau_j(\lambda)$ are the transmissions functions of interference filters used by each cameras (j = 1,2). Thus, the aim of the method is to find the photon flux I_{WI} [ph/m^2 s^{-1} sr^{-1}]:

$$I_{WI} = \int L_\lambda d\lambda \quad (3)$$

where L_λ is a shape function describing the shape of the emission line.

Hence, the photon passband flux behind the interference filter is:

$$\int L_\lambda \cdot \tau_j(\lambda) d\lambda = \frac{S_j}{K_j} - \int S_{brems}(\lambda) \cdot \tau_j(\lambda) d\lambda \quad (4)$$

Taking into account that $S_{brems}(\lambda)$ does almost not change within the filter bandwidth and the linewidth of the WI emission is much smaller in comparison with the bandwidths of the interference filters, Eq. (4) can be rewritten as:

$$T_j \int L_\lambda d\lambda = \frac{S_j}{K_j} - S_{brems}(\lambda_0) \cdot \int \tau_j(\lambda) d\lambda, \quad (5)$$

where T_j are the filter transmittances at the central wavelength of the tungsten emission line:

$$T_j = \tau_j(\lambda_0) = \frac{\int L_\lambda \cdot \tau_j(\lambda) d\lambda}{\int L_\lambda d\lambda}, \quad (6)$$

From Eq. (5) and using the approximation introduced by Eq. (6), one obtains the total photon flux of the respective emission line:

$$\int L_\lambda d\lambda = \frac{S_j}{K_j \cdot T_j} - S_{brems}(\lambda_0) \cdot \frac{\int \tau_j(\lambda) d\lambda}{\tau_j(\lambda_0)} = \frac{S_j}{K_j \cdot T_j} - S_{brems}(\lambda_0) \cdot \Delta\lambda_j \quad (7)$$

where $\Delta\lambda_j$ is the filter effective bandwidth:

$$\Delta\lambda_j = \frac{\int \tau_j(\lambda) d\lambda}{\tau_j(\lambda_0)} \quad (8)$$

From Eq. (7) and from the fact that the term on the left hand side $\int L_\lambda d\lambda$ is the same when calculated for either camera, the bremsstrahlung background can be expressed in terms of parameters, S_1, and S_2 as well as T_1, T_2, $\Delta\lambda_1$ and $\Delta\lambda_2$:

$$S_{brems}(\lambda_0) = \left(\frac{S_2}{K_2 \cdot T_2} - \frac{S_1}{K_1 \cdot T_1} \right) / (\Delta\lambda_2 - \Delta\lambda_1) \quad (9)$$

Substituting this S_{brems} (λ_0) into Eq. (7) one obtains for the total photon flux of the respective emission line W I:

$$I_{WI} = \int L_\lambda \cdot d\lambda = \left(\frac{S_1}{K_1 \cdot T_1} \cdot \Delta\lambda_2 - \frac{S_2}{K_2 \cdot T_2} \cdot \Delta\lambda_1 \right) / (\Delta\lambda_2 - \Delta\lambda_1) \quad (10)$$

This method will fail in the case of using the interference filters with identical effective bandwidth ($\Delta\lambda_1 = \Delta\lambda_2$), therefore only appropriate filters with different bandwidth ($\Delta\lambda_1 \neq \Delta\lambda_2$) should be used. The effective bandwidths of IFs used in this contribution and shown in Fig. 2a are $\Delta\lambda_1$ = 1.5 nm and $\Delta\lambda_2$ = 1.05 nm; they fulfil this requirement.

In the case of $S_{brems}(\lambda_0) = 0$, the Eqs. (9) and (10) give

$$I_{WI} = \frac{S_2}{K_2} \cdot \frac{1}{T_2} = \frac{S_1}{K_1} \cdot \frac{1}{T_1} \quad (11)$$

which shows that both spectral channels measure identical total photon fluxes of W I spectral line. It demonstrates also that Eq. (10) gives a sensible expression for the attached plasma conditions when there is no plasma continuum background.

2.2. Method for stretching images to match pixels

The method for extraction of WI emission line is based on pixel-wise comparison of the two recorded images taken by two cameras with the same field of view (FoV) and IFs of different FWHMs. Since the images from the cameras are in general slightly misaligned and modified by the individual filters optical properties, there is a need to correct one of them to match the other. This correction is performed by a spatial transformation where each point (*x, y*) of image A is mapped to a point (*x'*, *y'*) in a new coordinate system. The transformation is a composition of translation and rotation and which could be described in terms of matrix operations:

$$\begin{bmatrix} x' \\ y' \\ 1 \end{bmatrix} = \begin{bmatrix} 1 & 0 & x_{trans} \\ 0 & 1 & y_{trans} \\ 0 & 0 & 1 \end{bmatrix} \cdot \begin{bmatrix} cos\theta & -sin\theta & 0 \\ sin\theta & cos\theta & 0 \\ 0 & 0 & 1 \end{bmatrix} = \begin{bmatrix} cos\theta & -sin\theta & x_{trans} \\ sin\theta & cos\theta & y_{trans} \\ 0 & 0 & 1 \end{bmatrix} \quad (12)$$

where θ is the rotation angle about the origin (0;0) and (x_{trans}, y_{trans}) are translation values.

The optimal rotation matrix is found with help of a Kabsch algorithm. The Kabsch algorithm [24] is a method for calculating the optimal rotation matrix that minimizes the RMSD (root mean squared deviation) between two paired sets of points. The algorithm only computes the rotation matrix, but it also requires the computation of a translation vector.

3. Experimental results

The identification of the tungsten atom sources and the measurement of their radiation distribution in front of all plasma-facing components has been performed in JET-ILW with help of the mirror based endoscope system. This endoscope, equipped with four digital CCD cameras, covers the spectral range from 390 nm to 2500 nm with a high optical transmittance (≥20% in the near-UV wavelength range) as well as a high spatial resolution, that is is ≤ 2 mm at the object plane. Two digital cameras were used with identical two-dimensional views and with interference filters of different bandwidths centred on the W I (400.88 nm) emission line installed in front of the photocathode. They measured simultaneously the W I-emission profiles in the divertor region. A newly developed algorithm for the subtraction of the continuum radiation was successfully applied to evaluate the W emission for three different magnetic configurations as shown in Fig. 3. Each row in this figure represents the measurements of both cameras, results of the pure WI photon emission after the subtraction of the plasma continuum and configuration for the individual experiment. The neutral tungsten emission line is localised in the vicinity of the strike points. On the other hand, bremsstrahlung radiation takes place across the entire plasma volume due to Coulomb interactions as free electrons decelerate in the electric field of an ion. The bremsstrahlung intensity is $P_{brem} \sim n_e^2 Z_{eff} T_e^{-1/2}$ [25] with the main contribution attributed to the cool and dense divertor plasma region. Likewise, the contribution from free-bound recombination radiation is also localised to colder and denser plasma regions. The strong emission recorded from the inner divertor originates mainly from bremsstrahlung with significant fraction of the free-bound recombination radiation. The W I emission is the minor contributor to the radiation in the cold inner divertor. In the outer divertor the "halo" emission around the neutral tungsten emission is bremsstrahlung. Fig. 3 shows the successful evaluation of WI emission in front of the target in the outer divertor.

The experiment shown in Fig. 3a was designed to provide ELM-induced melting of the W lamellae in the divertor and has been performed in single null plasma discharges in deuterium with plasma currents I_p = 3.0 MA and toroidal magnetic field B_T ≈2.9 T. Fig. 4 shows the time evolution of this high energy confinement mode (H-mode) discharge in JET-ILW with an additional input power of $P_{IN} = P_{NBI} + P_{ICRH}$ = 20 MW + 1.5 MW = 21.5 MW. It demonstrates a stored energy of 5.5 MJ as well as regular type I ELMs with an ELM energy loss of ΔW_{ELM} = 0.2 MJ and an ELM frequency of f_{ELM} = 38 Hz during the flattop phase of the plasma discharge. Obviously, the time resolution of the recording camera systems of 30.5 ms was insufficient to resolve the ELMs. Furthermore, in the case shown in Figs. 3a and 4, the ELM frequency was not low enough (below 30 Hz) to record at the same time the contribution of one single ELM and an image without any ELM contribution. Every video frame contains the contribution of at least one ELM. Therefore, the inter-ELM W source information in this case is obtained with the help of a PhotoMultiplier Tube (PMT) system, which collects the light in the wavelength range of 395–409 nm from

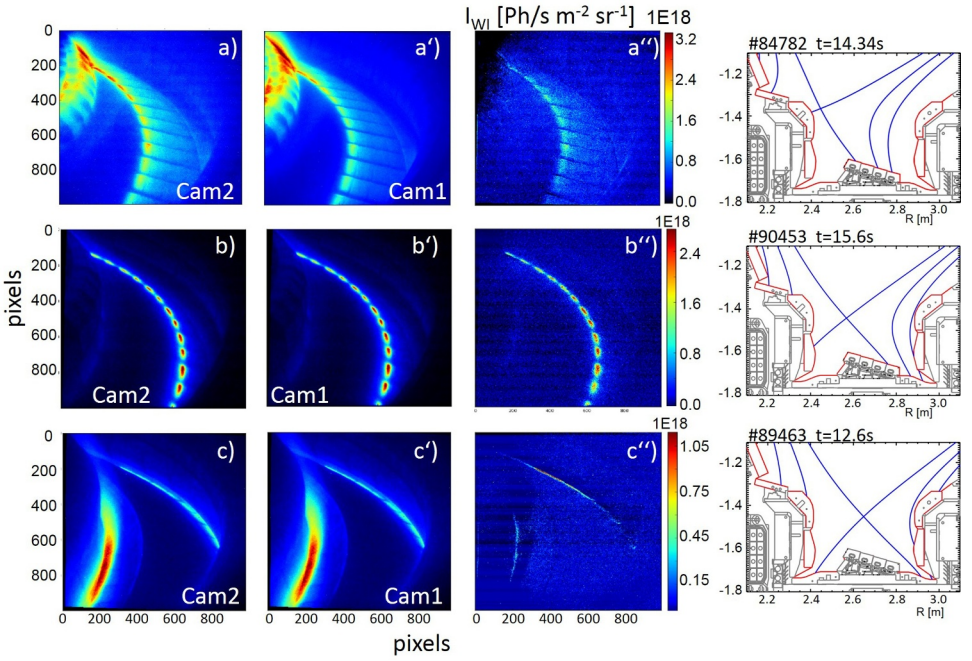

Fig. 3. W I -emission profiles in the divertor region taken simultaneously by two camera systems with the same two-dimensional view (Fig.3a and a', Fig.3b and b', Fig.3c, and c') during the experiment in JET with different magnetic field configurations. The figures a'', b'' and c'' show the result of the WI photon emission after the subtraction of the plasma continuum for these three configurations. Each row represents the measurements, results and configuration for the individual experiment.

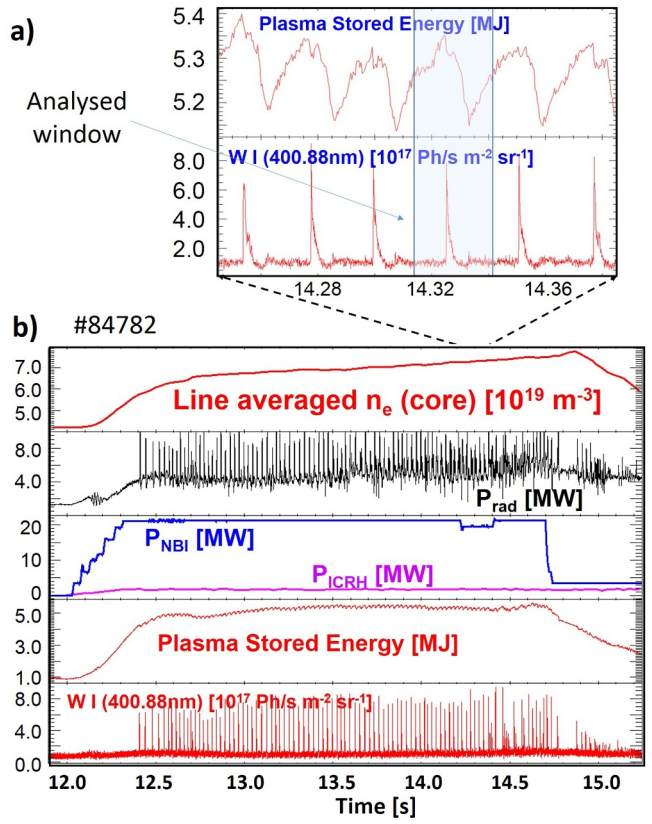

Fig. 4. Time evolution of an H-mode discharge with additional input power of 21.5 MW, a stored energy of 5.5 MJ as well as regular type I ELMs at ELM energy loss of ΔW_{ELM} = 0.2 MJ and ELM frequency of f_{ELM} = 38 Hz.

the outer target (Fig. 4, WI emission signal). Light is relayed by fibre optics to the PMT equipped with 400.9 nm bandpass filters (1 nm bandwidth), providing a time response of up to 10 kHz. Based on the fast PMT measurement, the inter-ELM induced sputtering amounts to 3.75×10^{19} atoms/s integrated over the entire outer strike point. Based on T_e probe measurements of 15 eV at the outer strike point, the *S/XB* value of 25 is used here [14]. The inter-ELM saturation current for the outer divertor amounts to 2.2×10^{23} el/s relating the tungsten flux to a sputtering yield of 1.7×10^{-4}. The measured sputtering yield is similar to the L-mode results reported in [10]. It states in [10] that a fraction of 0.5% beryllium in the target flux density is sufficient to explain the observed tungsten sputter signal. Taking into the account the findings in [10] that sputtering during ELMs dominates over in-between ELM sputtering by a factor of 5–10, the algorithm for the subtraction of the continuum is applied to evaluate the ELM-resolved W source. The measured number of photons emitted by neutral tungsten integrated over the entire outer strike point of a single module (not resolved) amounts to 2.9×10^{15} ph/ELM. Assuming that the WI emission from each module (48 modules in JET-ILW) is the same, we will get the total number of emitted WI photons of 1.4×10^{17} ph/ELM from the entire outer divertor. During the ELMs, an electron temperature of 70–100 eV at the strike point is assumed, giving *S/XB* values of about 50 leading to an intra-ELM sputtering of about 7×10^{18} atoms/ELM, in good agreement with the PMT measurements ($\approx 6 \times 10^{18}$ atoms/ELM). For the PMT measurements, the signal has been integrated over the time duration of the analysed ELM to get the total number of the emitted WI photons, and the geometry of the PMT line-of-sight (LOS) has been taken into the account. Given the 38 Hz ELM frequency, this confirms the original assumption that intra-ELM sputtering dominates by a factor of 7 over inter-ELM sputtering.

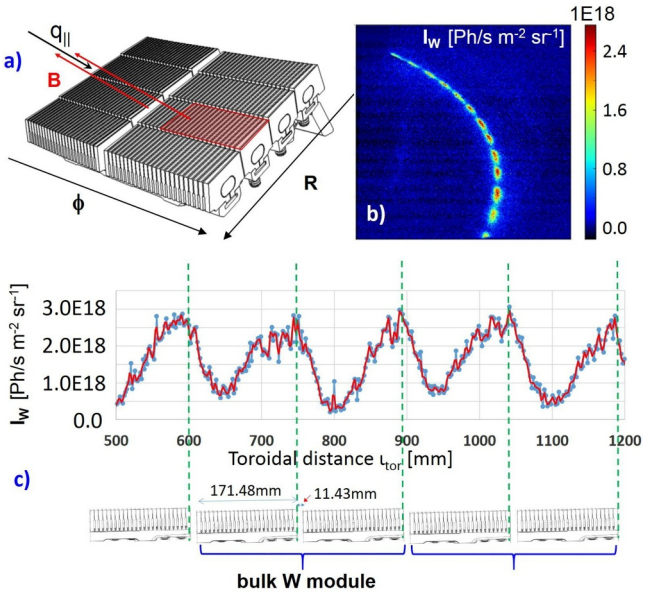

Fig. 5. Full view of a bulk W module (a) with indication of the wetted area, divertor view (b) as seen by the AVT-PIKE camera (KL11) equipped with a WI interference filter; toroidal distribution of the photon flux I_{WI} at the outer strike point measured in discharge JPN 90453 at t = 55.599 s (c).

Fig. 3b shows evaluation of the W I emission for a L-mode discharge in JET-ILW with ICRH heating alone. The inner strike point was located on the inner vertical target and the outer strike point on the horizontal target, tile 5 stack C. The continuous ICRH heating power of about 1 MW has been provided by successive operation of individual antennae. When one of the antennae was turned off, the other one was turned on to provide a continuous constant heating power of 1 MW. Thus only a single antenna was in operation at once. The plasma current varied from 1.77 MA to 2.5 MA at constant B_T= 2.4 T. While turning off the antenna, a transient erosion of the tungsten has been observed at the outer strike point. Recorded videos of the W I emission (Fig. 3b and b') have been analysed and the result presented on the Fig. 3b" . One sees a strong localised emission of the neutral W in front of the target.

Fig. 5 shows a full view of a bulk W module, which consists of two tiles. The plasma-facing tungsten tile is segmented in both the toroidal and poloidal directions. Each tile (96 of them in total, distributed in 48 modules) consists of four stacks of 24 tungsten blades each [27]. The thickness of these lamellae, in the toroidal direction, is about of 6 mm and the gap width between lamellae in a stack is 1 mm. The gap between tiles on a single module is 11.43 mm, and the gap between modules is 13.65 mm. The fraction of the wetted area where the heat and particle fluxes are deposited is of about 0.74 at the time event of the measurement shown in Fig. 5b. The angle of incidence of the field lines in the sectional plane (elevation) is $\theta_\perp = 1.9^\circ$. The Fig. 5b and c show the variation of the emission of the neutral tungsten in toroidal direction with strong correlation with the wetted area and the maximum radiation at the edge of the divertor tile. There appears to be a strong WI emission from an area of the divertor surface that is shadowed by the neighbouring bulk W module (just to the right of each vertical dotted green line). This is due to the observation geometry of the cameras as well as to the finite ionisation length of the sputtered W atoms. It has no impact on the measurements of the W influx because the WI emission light from the entire divertor module is collected. The maximal value of photon fluxes measured at the edges of the module tiles amounts to about 2.5×10^{18} ph/s/m^2 sr^{-1}. Langmuir probe measurements were used to determine profiles of the divertor plasma

temperature, delivering the value of $T_e = 20$ eV at the outer strike point during the erosion events. The *S/XB* value for such electron temperatures is of about 30 [14,26]. The sputtering caused by this transient event was 3×10^{18} atoms/event, which is comparable to the ELM sputtering reported above.

The result achieved from the experiment in the corner configuration Fig. 3c) demonstrates the effective application of this method for the evaluation of the W erosion even in the inner divertor region where the strong recombination emission is dominating over the tungsten emission. Recorded videos were obtained from an H-mode discharge (JET Pulse No: 89463) with auxiliary heating of 12.0 MW directly after the L-H transition during the ELM-free phase in magnetic equilibria: $B_T \approx 2.8$T, $I_p = 2.5$ MA, $q_{95} = 3.26$. The operation has been performed in the static corner configuration. In such corner configurations the strike points are only partially visible due the shadowing of the vertical tiles. The emission of the neutral tungsten can be seen only at the inner and outer strike points which can be viewed. At the same time, the emission does not appear in the area where the strike points are shadowed by vertical tiles, demonstrating the correctness of this method. After subtraction, the background in the inner divertor is not fully compensated due the parasitic light scattering on the mirror optics, which is not fully identical for both these cameras. The non-compensated background is about of 12–17% of the W I emission signal. The compensation procedure of this parasitic light is under development and is not included in the present contribution. Taking into the account the parasitic light compensation could further improve the measurements in the inner divertor. The in-out asymmetry of the photon flux I_{WI} integrated over the same area in the inner and outer divertor regions is about 1:3. The inner divertor is at least partially detached with the measured T_e^{ISP} of about 3 eV close to the inner strike point. On the other hand, the electron temperature close to the outer strike point, measured by Langmuir probes again, is about $T_e^{OSP} = 20$ eV. As show in [13,26] the *S/XB* -factor which relates particle and photon flux is strongly temperature dependent: $S/XB = 5$ for $T_e^{ISP} = 3$ eV and $S/XB = 30$ for $T_e^{OSP} = 20$ eV . Taking into account these *S/XB* values, the in-out asymmetry of W atom influxes can be calculated by using the formula ((1):

$$\frac{\Gamma_W{}^{inner}}{\Gamma_W{}^{outer}} = \frac{\frac{S}{XB}(T_e = 5eV)}{\frac{S}{XB}(T_e = 20eV)} \cdot \frac{I_{WI}{}^{inner}}{I_{WI}{}^{outer}} = 1:18 \tag{13}$$

It should be mentioned here that this asymmetry is not constant and depends strongly on the conditions and plasma parameters such as T_e at the strike points and in the divertor legs. This result is consistent with previous findings [10,26] in the outer divertor considering that in-between ELMs deuterium ions have too low energy for tungsten sputtering and thus only beryllium impurity ions lead to tungsten erosion. However, as demonstrated here, during the inter-ELM phase even the beryllium ion impact energies can become too low to sputter the tungsten in the inner divertor area. Calculated physical sputtering yields of W by Be are below 10^{-4} at Be ion energies below 65 eV [20]. Taking into the account (i) the strong in/out divertor asymmetry (e.g. asymmetry in n_e, T_e, heat loads) in JET-ILW L-mode plasmas as well as during the inter-ELM phases and (ii) the fact that the inner divertor is almost always at least partially detached, we can confirm that the outer divertor tiles are dominating areas for W erosion in the inter-ELM phase. However, it should be mentioned here that the situation changes during the ELM phase. During ELMs tungsten sputtering due to deuterium becomes important and even can dominate, which could lead to significant W erosion in the outer as well as in the inner divertor. This was confirmed in [26] showing that during ELMs the outer divertor W source is larger than the inner one by a factor of 1.8 only.

Conclusions

The identification of the tungsten atom sources and the measurement of their radiation distribution in front of all plasma-facing components has been performed in JET with the help of an endoscope equipped with four digital CCD cameras, each combined with filter wheels for narrow-band interference and neutral density filters. This diagnostic system provides the same two-dimensional view simultaneously for different spectral lines. The scope of this contribution is to provide a clean image of the single spectral line of tungsten by using two camera images with interference filters of different bandwidths centred on the W I (400.88 nm) emission line. A new algorithm for the subtraction of the continuum radiation was successfully developed and is now used to evaluate the W erosion even in the inner divertor region where the strong recombination emission is dominating over the tungsten emission. It should be mentioned here that this technique is not necessarily required for typical attached conditions. Contrary to the attached conditions, this technique is mandatory for the semi-detached or fully detached divertor conditions as well as high radiative seeding scenarios.

Additionally, analysis of W sputtering and W redistribution in the divertor by video imaging spectroscopy with high spatial resolution for three different magnetic configurations was presented. The resultant intra-ELM sputtering was of about 7×10^{18} atoms/ELM in the experiments with 3 MA/2.9 T high energy confinement mode (H-mode) pulses and an input power of $P_{IN} = 21.5$ MW, a stored energy of 5.5 MJ as well as regular type I ELMs at ELM energy loss of $\Delta W_{ELM} = 0.2$ MJ and ELM frequency of $f_{ELM} = 38$ Hz. Given the 38 Hz ELM frequency, this implies that intra-ELM sputtering dominated by a factor of 7 over inter-ELM sputtering. This result is consistent with previous finding in JET-ILW [10,26] and ASDEX Upgrade [28] that intra-ELM erosion dominates the total W source. The intra-ELM source varied strongly, by one order of magnitude, depending on the ELM energy loss while the inter-ELM source remained approximately the same.

The results achieved from the experiment in the corner configuration (Fig. 3c) demonstrate the effective application of this method for the evaluation of the W erosion even in the inner divertor region where the strong recombination emission is dominating over the tungsten emission. The inter-ELM tungsten atom fluxes were found to be strongly asymmetric, with the outer divertor favoured by a factor of 18, thus making the outer divertor tiles dominating W erosion areas for the inter-ELM phase.

The tungsten erosion distribution in the divertor has been measured in an L-mode plasma discharge with an additional heating power of $P_{ICRH} = 1$ MW. Strong variation of the emission of the neutral tungsten in toroidal direction and corresponding W erosion has been observed. It strongly correlates with the wetted area with maximum W erosion at the edge of the divertor tile. The measured sputtering yield of 1.7×10^{-4} is consistent with the L-mode results reported in [10]. The observed tungsten sputter signal cannot be explained by deuterium ions as the only sputtering species. It could be explained by a fraction of $\approx 0.5\%$ beryllium in the target flux density, which is the dominant impurity in the plasma, leading to the conclusion that the tungsten erosion during the L-mode plasma as well as during the inter-ELM phase is mainly caused by beryllium.

Acknowledgements

This work has been carried out within the framework of the EUROfusion Consortium and has received funding from the Euratom research and training programme 2014–2018 under grant agreement No 633053. The views and opinions expressed herein do not necessarily reflect those of the European Commission.

References

[1] 13th ITER Council 20â€“21 November 2013.
[2] R.A. Pitts, S. Carpentier, F. Escourbiac, et al., J. Nucl. Mater. 438 (2013) 48.
[3] G. JaneschitzITER JCT and HTs, J. Nucl. Mater. 290–293 (2001) 1.
[4] H.D. B Jenkins and H.K. Roobottom 2004 CRC Handbook of Chemistry and Physics 85th ed. (Boca Raton, FL: CRC Press).
[5] T. Hirai, Phys. Scr. T103 (2003) 59.
[6] O. Ogorodnikova, et al., J. Nucl. Mater. 313–316 (2003) 469.
[7] T. Pütterich, et al., Nucl. Fusion 50 (2010) 025012.
[8] J.W. Coenen, et al., Nucl. Fusion 53 (2013) 073043.
[9] H. P. Summers et al., At. Data Anal. Struct., URL: http://www.adas.ac.uk/.
[10] G.J. van Rooij, et al., J. Nucl. Mater. 438 (2013) S42.
[11] K. Behringer, et al., Plasma Phys. Control. Fusion 31 (1989) 2059.
[12] A. Pospieszczyk, et al., J. Phys. B: At. Mol. Opt. Phys. 43 (2010) 144017.
[13] M. Laengner, et al., J. Nucl. Mater 438 (2013) S865.
[14] S. Brezinsek, et al., Phys. Scr. T170 (2017) 014052.
[15] T. Abrams, et al., Nucl. Mater. Energy 17 (2018) 164.
[16] G. Sergienko private communication.
[17] T. Abrams, et al., IEEE Trans. Plasma Sci. 46 (N○. 5) (2018) 1298.
[18] O. Meyer, et al., Rev. Sci. Instrum. 89 (2018) 10D105.
[19] G.F. Matthews, et al., Phys. Scr. T145 (2011) 014001.
[20] S. Brezinsek, et al., J. Nucl. Mater. 463 (2015) 11.
[21] A. Huber, et al., Rev. Sci. Instrum. 83 (2012) 10D511.
[22] A. Huber A, et al., Fusion Eng. Des. 88 (2013) 1361.
[23] T.M. Biewer, et al., Rev. Sci. Instrum. 83 (2012) 10D505.
[24] W. Kabsch, A solution for the best rotation to relate two sets of vectors, Acta Crystallographica A32 (1976) 922, https://doi.org/10.1107/S0567739476001873.
[25] A.T. Ramsey, S.L. Turner, Rev. Sci. Instrum. 58 (1987) 1211.
[26] N. Den Harder, et al., Nucl. Fusion 56 (2016) 026014.
[27] P.h. Mertens, et al., Phys. Scr. T145 (2011) 014002.
[28] R. Dux, et al., J. Nucl. Mater. 390–391 (2009) 858.